



Engineering Sciences & Applications Division
Applied Engineering Technologies

To/MS: Seppo Penttila, P-23, H803
Thru: Coyne Prenger, ESA-AET, J580
From/MS: Todd Jankowski, ESA-AET, J580
Phone/Fax: (505) 667-5735/Fax (505) 665-7740
Symbol: ESA-AET:05-28
Date: December 17, 2004

SUBJECT: Transient Analysis of Hydrogen Discharge from the NPDGamma Target Vessel.

I. Summary

This document presents an analysis of hydrogen venting after a failure of the 21 L liquid hydrogen (LH2) target vessel used in the NPDGamma project. Calculations are performed using relief line geometries for the target installed in the shed at MPF-35 and for the target installed in ER-2. For each of these relief line geometries, simulations are performed for a case when the 20 psig rupture disk opens and allows hydrogen vapor to flow through the relief line, and for a case when the 20 psig rupture disk fails to open and the 30 psig rupture disk must be used for venting. In all cases, the analyses show that the relief pipes are sized large enough to prevent the generation of excessive pressure levels in the vacuum vessel.

II. Introduction

The formulation and results of a transient numerical analysis of hydrogen discharge after a rupture of the LH2 target vessel used in the NPDGamma project are presented here. The analysis assumes that, after a target vessel rupture, 21 L of LH2 spill into the vacuum space surrounding the target vessel. The hydrogen is then subjected to a heat load from the ambient, resulting in a pressure rise in the vacuum vessel. The pressure of the hydrogen in the vacuum vessel increases until the burst pressure of a rupture disk is reached. After a rupture of the disk, hydrogen vapor flows through the relief piping and is discharged to the atmosphere. Two distinct relief piping geometries are analyzed here. We consider the cases when (1) the LH2 target is installed in the shed at MPF-35, and (2) the LH2 target is installed in ER-2. In each case, simulations are performed for a rupture of the primary (20 psig) rupture disk and for a case when the primary rupture disk fails to open and we must rely on the secondary (30 psig) rupture disk for venting. The system geometry and operating conditions are given in Section III. In Section IV, assumptions used in the model are presented. Section V outlines the governing equations used to model the hydrogen discharge. Results of the hydrogen discharge simulations are then given in Section VI, followed by conclusions in Section VII.

III. Geometry and Operating Conditions

The equations used in the analysis are applied to the system illustrated in Figure 1. Hydrogen temperature, pressure, density, and velocity are calculated at discrete points or nodes in the system. The vacuum vessel is treated as one node in the model, while five nodes are included in the relief pipe. Detailed drawings of the target vessel, vacuum vessel, and relief piping can be found in the NPDGamma Liquid Hydrogen Target Engineering Document.¹ The relief pipe geometry listed in Table 1 has been determined after reviewing the drawings in the engineering document for the system installed in MPF-35 and in ER-2. Listed in the table are lengths (Δx), hydraulic diameters (D_h), and elevation changes (Δz)

for sections of the relief pipe between each node modeled in the system. In addition, the table lists valves and fittings that are used in each section of the relief pipe. The flow resistance through valves and fittings are modeled using either loss coefficients (K) or equivalent lengths of straight pipe (L_e/D). The values used for loss coefficients and equivalent lengths for elbows, tees, the square-edged entrance, and the check valve are obtained from the text of Fox and McDonald.² The rupture disks used in the system are Fike model SR-H rupture disks with a reported $K = 1.88$.³ Here, however, we use a more conservative value suggested by the ASME boiler and pressure vessel code of $K = 2.4$.⁴

We assume that before the target vessel ruptures, it is filled with 21 L of saturated liquid hydrogen at a pressure of 1 atm. The vacuum vessel has a total volume of 170 L and a surface area (exposed to ambient air) of 2 m². After the target vessel rupture, we assume that the hydrogen in the vacuum vessel and the relief pipe are absorbing a heat flux (q'') from the ambient.

IV. Assumptions

The target vessel rupture and hydrogen venting is a three-step process. First, after the vessel ruptures, the 21 L of LH2 expands to fill the 170 L vacuum space. Second, with the rupture disks closed, the hydrogen absorbs heat from the wall of the vacuum vessel, resulting in a pressure rise in the constant volume vacuum space. Third, the rupture disk ruptures, resulting in a flow of hydrogen out of the relief line. The assumptions used to model each of these processes are:

1. *Expansion from the target vessel to the vacuum space.*
 - a. The expansion process is isentropic.
2. *Constant volume heat addition.*
 - a. The entire inner surface of the vacuum vessel is covered with liquid and maintained at ambient temperature. A film boiling heat flux for hydrogen is used.
3. *Flow through the relief line.*
 - a. The entire inner surface of the vacuum vessel is covered with liquid and maintained at ambient temperature. A film boiling heat flux for hydrogen is used.
 - b. The fluid entering the relief pipe is saturated vapor.
 - c. The surface temperature of the piping is maintained at ambient temperature.
 - d. The flow in the relief piping is fully turbulent.

The assumptions listed here will result in a conservative (high) estimate of the maximum pressure generated in the vacuum space after a failure of the target vessel. Modeling the expansion process as an ideal isentropic process will maximize the amount of liquid present in the vacuum space. Any real expansion process will involve heat transfer from the ambient to the hydrogen as well as frictional losses as the hydrogen flows from the target vessel into the vacuum space. Both the friction and the heat transfer will increase the entropy and the vapor fraction compared to the ideal process. Modeling the heat transfer to the hydrogen in the vacuum vessel and relief piping as heat transfer with a boundary temperature equal to the ambient ignores the effects of conduction through the walls of the vacuum vessel and relief piping, convection through the surrounding air, and the thermal mass of the vacuum vessel and relief piping. Ignoring these thermal resistances results in higher heat transfer rates than would actually be present in the system. Additionally, in the vacuum vessel, we ignore the presence of vapor, and assume that the entire surface of the vacuum vessel is absorbing the film boiling heat flux. Film boiling is a much more

efficient heat transfer process than natural convection through vapor, resulting in an overestimate of the heat flux to the vacuum vessel. Overestimating the heat transfer rates to various components in the system will overestimate the pressure in the vacuum vessel by increasing the boil-off rate of hydrogen in the vacuum vessel and by increasing the likelihood of thermal choking in the relief piping.

V. Governing Equations

A. Isentropic Expansion

Before the isentropic expansion, the hydrogen is confined to the target vessel with a volume $(V_1)^0 = 21$ L, a pressure $(P_1)^0 = 1$ atm, and a quality $(x_1)^0 = 0$. The initial pressure and quality define the state of the fluid, and an equation of state can be used to calculate the initial density $(\rho_1)^0$ and the initial entropy $(s_1)^0$. After the expansion process to $V_1 = 170$ L, the entropy is equal to the initial entropy (isentropic process), and the mass is equal to the initial mass. The entropy and density of the fluid after the isentropic expansion are then calculated from

$$\text{Isentropic process:} \quad s_1 = (s_1)^0 \quad (1)$$

$$\text{Mass balance:} \quad \rho_1 = \frac{(\rho_1 V_1)^0}{V_1}. \quad (2)$$

These two independent properties define the state of the hydrogen after the expansion process.

B. Constant Volume Heat Addition

With the rupture disk closed, the volume that the hydrogen occupies and the mass of hydrogen in the vacuum vessel are constant. Therefore, the density of hydrogen in the vacuum vessel, during the constant volume heat addition, does not change with time, or

$$\text{Mass balance:} \quad \frac{d\rho_1}{dt} = 0. \quad (3)$$

In addition, an energy balance for the closed system is given as

$$\text{Energy balance:} \quad \frac{dU_1}{dt} = \rho_1 V_1 \frac{du_1}{dt} = q_1'' A_{s,1}, \quad (4)$$

where U_1 is the internal energy of the hydrogen in the vacuum vessel, u_1 is the specific internal energy, q_1'' is the heat flux to the hydrogen in the vacuum vessel, and $A_{s,1}$ is the surface area of the vacuum vessel.

Using 1st order backward differences to discretize Eqs. (3) and (4), shows that

$$\text{Mass balance:} \quad \rho_1 = (\rho_1)^0 \quad (5)$$

$$\text{Energy balance:} \quad \rho_1 V_1 [u_1 - (u_1)^0] = q_1'' A_{s,1} \Delta t, \quad (6)$$

where Δt is the time step, and quantities with superscript 0 are evaluated at the previous time step. The final fluid state from the expansion process [calculated from Eqs. (1) and (2)] is used as an initial condition to the constant volume heat addition process [Eqs. (5) and (6)]. The mass and energy balance equations in Eqs. (5) and (6) allow for a determination of the state of the hydrogen at each time step (internal energy and density are two independent properties).

C. *Flow from the Vacuum Vessel Through the Relief Piping: Differential Equations*

The flow through the relief piping is modeled using the transient macroscopic mass, momentum, and energy balances.⁵ General forms of the balances used can be written as

$$\text{Mass: } \frac{dm}{dt} = \rho_i v_i A_{x,i} - \rho_{i+1} v_{i+1} A_{x,i+1} \quad (7)$$

$$\text{Momentum: } \frac{dM}{dt} = (\rho_i v_i^2 + P_i) A_{x,i} - (\rho_{i+1} v_{i+1}^2 + P_{i+1}) A_{x,i+1} - \frac{1}{2} (\rho_i A_{x,i} + \rho_{i+1} A_{x,i+1}) (z_{i+1} - z_i) g - F_b \quad (8)$$

$$\text{Energy: } \frac{d(KE + U)}{dt} = \rho_i A_{x,i} v_i \left(\frac{1}{2} v_i^2 + g z_i + h_i \right) - \rho_{i+1} A_{x,i+1} v_{i+1} \left(\frac{1}{2} v_{i+1}^2 + g z_{i+1} + h_{i+1} \right) + q''_{i \rightarrow i+1} A_{s,i \rightarrow i+1} \quad (9)$$

where i is an upstream spatial location, and $i+1$ is a downstream spatial location. The new variables appearing in Eqs. (7) through (9) are:

$A_{s,i \rightarrow i+1}$	Surface area of the control volume from i to $i+1$.	KE	Kinetic energy (defined below)
$A_{x,i}$	Cross-sectional area at location i .	m	Mass (defined below)
F_b	Boundary forces (defined below)	M	Momentum (defined below)
g	Acceleration due to gravity	P	Pressure
h	Specific enthalpy	v	Velocity
		z	Height measured from the vacuum vessel (positive upward)

The mass, momentum, kinetic and internal energy, and the boundary forces are defined as

$$m = \int \rho dV \quad (10)$$

$$M = \int \rho v dV \quad (11)$$

$$KE + U = \int \left(\frac{1}{2} \rho v^2 + \rho u \right) dV \quad (12)$$

$$F_b = \frac{1}{2} \rho_{i+1} v_{i+1}^2 A_{x,i+1} \left[f \left(\frac{\Delta x}{D_{h,i+1}} + \frac{L_e}{D} \right) + K_{i \rightarrow i+1} \right] - P_i (A_{x,i+1} - A_{x,i}) \quad (13)$$

where x is the spatial coordinate in the flow direction, Δx is the length of piping between points i and $i+1$, f is the Darcy friction factor, D_h is the hydraulic diameter, L_e/D is an equivalent length used to represent losses in valves and fittings, and K is a loss coefficient.

D. *Discrete Equations*

The differential equations written above are now discretized. To approximate the integrals in Eqs. (10) through (12), we assume that the upstream value of the mass, kinetic energy, and internal energy prevail over the length of the control volume Δx . This upwind scheme has been suggested for compressible flows by Karki and Patankar.⁶ Additionally, the volume element dV , in Eqs. (10) through (12), is expressed as

$$dV = \begin{cases} V_1 & \text{flow from vacuum vessel to relief pipe} \\ A_{x,i} \Delta x & \text{flow in the relief pipe} \end{cases} \quad (14)$$

Using the upwind scheme and Eq. (14), gives the integral approximations

$$m = \begin{cases} \rho_1 V_1 & \text{flow from vacuum vessel to relief pipe} \\ \rho_i A_{x,i} \Delta x & \text{flow in the relief pipe} \end{cases} \quad (15)$$

$$M = \begin{cases} \rho_1 v_1 V_1 = 0 & \text{flow from vacuum vessel to relief pipe} \\ \rho_i v_i A_{x,i} \Delta x & \text{flow in the relief pipe} \end{cases} \quad (16)$$

$$KE + U = \begin{cases} \left(\frac{1}{2} \rho_1 v_1^2 + \rho_1 u_1\right) V_1 = \rho_1 u_1 V_1 & \text{flow from vacuum vessel to relief pipe} \\ \left(\frac{1}{2} \rho_i v_i^2 + \rho_i u_i\right) A_{x,i} \Delta x & \text{flow in the relief pipe} \end{cases} \quad (17)$$

Now we use first-order backward differences to approximate the time derivatives, so that

$$\frac{dm}{dt} = \begin{cases} \left[\rho_1 - (\rho_1)^0\right] V_1 / \Delta t & \text{flow from vacuum vessel to relief pipe} \\ \left[\rho_i - (\rho_i)^0\right] A_{x,i} \Delta x / \Delta t & \text{flow in the relief pipe} \end{cases} \quad (18)$$

$$\frac{dM}{dt} = \begin{cases} 0 & \text{flow from vacuum vessel to relief pipe} \\ \left[\rho_i v_i - (\rho_i v_i)^0\right] A_{x,i} \Delta x / \Delta t & \text{flow in the relief pipe} \end{cases} \quad (19)$$

$$\begin{aligned} & \frac{d(KE + U)}{dt} \\ & = \begin{cases} \left[\rho_1 u_1 - (\rho_1 u_1)^0\right] V_1 / \Delta t & \text{flow from vacuum vessel to relief pipe} \\ \left[\frac{1}{2} \rho_i v_i^2 - \frac{1}{2} (\rho_i v_i^2)^0 + \rho_i u_i - (\rho_i u_i)^0\right] A_{x,i} \Delta x / \Delta t & \text{flow in the relief pipe} \end{cases} \end{aligned} \quad (20)$$

For the flow from the vacuum vessel (node 1) into the relief pipe (node 2), the hydrogen in the vacuum vessel is stagnant, so that $v_1 = 0$. The discrete forms of the governing equations for the flow from the vacuum vessel to the relief piping are given by

$$\text{Mass:} \quad \left[\rho_1 - (\rho_1)^0\right] = -\rho_2 v_2 A_{x,2} \Delta t / V_1 \quad (21)$$

$$\text{Momentum:} \quad P_1 = (1 + K_{1 \rightarrow 2} / 2) \rho_2 v_2^2 + P_2 \quad (22)$$

$$\text{Energy:} \quad \left[\rho_1 u_1 - (\rho_1 u_1)^0\right] = \left[\rho_1 - (\rho_1)^0\right] \left(\frac{1}{2} v_2^2 + h_2\right) + q_1'' A_{x,1} \Delta t / V_1 \quad (23)$$

where Eq. (21) has been used to simplify the energy equation, and the momentum equation has been obtained by letting $A_{x,1} = A_{x,2}$.

The discrete forms of the time derivatives can also be substituted into the governing differential equations to obtain the discrete equations describing the flow in the relief pipe. After the substitutions are made we have

$$\text{Mass:} \quad \left[\rho_i - (\rho_i)^0\right] \Delta x / \Delta t = \rho_i v_i - \rho_{i+1} v_{i+1} \left(D_{h,i+1} / D_{h,i}\right)^2 \quad (24)$$

$$\begin{aligned} \text{Momentum:} \quad & \left[\rho_i v_i - (\rho_i v_i)^0\right] \Delta x / \Delta t = \rho_i v_i^2 - \left(\rho_{i+1} v_{i+1}^2 + P_{i+1} - P_i\right) \left(D_{h,i+1} / D_{h,i}\right)^2 \\ & - \frac{1}{2} \left[\rho_i + \rho_{i+1} \left(D_{h,i+1} / D_{h,i}\right)^2\right] (z_{i+1} - z_i) g - \frac{1}{2} \rho_{i+1} v_{i+1}^2 \left(D_{h,i+1} / D_{h,i}\right)^2 \left[f \left(\Delta x / D_{h,i+1} + L_e / D\right) + K_{i \rightarrow i+1}\right] \end{aligned} \quad (25)$$

$$\text{Energy: } \left[\frac{1}{2} \rho_i v_i^2 - \frac{1}{2} (\rho_i v_i^2)^0 + \rho_i u_i - (\rho_i u_i)^0 \right] \Delta x / \Delta t = \rho_i v_i \left(\frac{1}{2} v_i^2 + g z_i + h_i \right) - \rho_{i+1} v_{i+1} \left(\frac{1}{2} v_{i+1}^2 + g z_{i+1} + h_{i+1} \right) \left(D_{h,i+1} / D_{h,i} \right)^2 + 4 q_{i \rightarrow i+1}'' \frac{\Delta x}{D_{h,i}}, \quad (26)$$

which are obtained after recognizing that for the round cross-section of relief pipe, $A_{x,i} = \pi D_{h,i}^2 / 4$ and $A_{s,i \rightarrow i+1} = \pi D_{h,i} \Delta x$.

The friction factor is calculated using the formula of Swamee and Jain,⁷

$$f = 0.25 \left[\log \left(5.74 / \text{Re}_{i+1}^{0.9} \right) \right]^{-2}, \quad (27)$$

which is an asymptotic approximation to the Colebrook equation. The expression listed in Eq. (27) assumes smooth tubes. The Reynolds number appearing in Eq. (27) is defined as

$$\text{Re}_{i+1} = \rho_{i+1} v_{i+1} D_{h,i+1} / \mu_{i+1}, \quad (28)$$

where μ_{i+1} is the dynamic viscosity of the fluid at location $i+1$.

The heat flux to the fluid flowing in the relief pipe is calculated from Newton's law of cooling

$$q_{i \rightarrow i+1}'' = H \left(T_{s,i \rightarrow i+1} - T_{b,i \rightarrow i+1} \right), \quad (29)$$

where H is the heat transfer coefficient, T_s is the temperature of the inner surface of the relief pipe (taken to be 300 K), and $T_{b,i \rightarrow i+1} = \frac{1}{2} (T_{i+1} + T_i)$ is an average bulk temperature of the fluid flowing from i to $i+1$.

The heat transfer coefficient is estimated using the Dittus-Boulter equation for turbulent flow in tubes,⁸

$$H = \frac{k_b}{D_{h,i}} 0.23 \text{Re}_i^{0.8} \text{Pr}_b^{0.4}, \quad (30)$$

where k_b and Pr_b are the thermal conductivity and Prandtl number of the gas, respectively. Both properties are evaluated at the bulk fluid temperature.

E. Programming

The system of algebraic equations outlined above were programmed in Engineering Equation Solver (EES) software.⁹ The built-in equation of state for hydrogen in EES was used to calculate all of the fluid properties needed in the model.^{10,11} EES uses Newton's method to iteratively solve systems of non-linear algebraic equations. Because of this capability in EES, linearization of the discrete equations is not required before attempting a solution. The equations presented in Section V (A-D) are directly written into and solved by the program.

VI. Results

The results of the isentropic expansion and constant volume heat addition processes are shown in Figures 2 through 4. Figure 2 is a temperature-entropy (T-S) diagram of these processes. As illustrated in the figure, the process begins with saturated liquid in the target vessel. After the target vessel rupture, an isentropic (constant entropy) expansion reduces the pressure and temperature of the hydrogen. The expansion process is followed by the constant volume heat addition process (notice that the line on the process diagram follows a line of constant specific volume). In Figure 3, the pressure in the vacuum vessel is shown as a function of time. From the figure, we see that after 1.4 seconds, the 20 psig burst pressure of the primary rupture disk is reached. If the 20 psig rupture disk fails to open, the burst pressure

of the secondary (30 psig) rupture disk will be reached in 1.7 seconds. Figure 4 presents the volume fraction of vapor (or ullage) in the vacuum vessel versus time. The isentropic expansion process produces 90 % vapor in the vacuum vessel. Additional vapor is then produced during the constant volume heat addition process.

Figures 5 through 9 present the results for the target vessel installed in ER-2 after the 20 psig rupture disk opens. In Figure 5, hydrogen pressure is plotted as a function of time for each of the six nodes in the system. From the figure, notice that as soon as hydrogen starts flowing out of the relief line (after the rupture disk opens at 1.4 seconds) the pressure in the vacuum vessel decreases. This is a significant result, showing that the capacity of the relief line is adequate to handle the hydrogen discharge after a failure of the target vessel. The hydrogen temperature at each node in the system is shown in Figure 6. The figure shows the effect that the heat load to the un-insulated relief lines has on the hydrogen temperature. In Figure 7, the Mach numbers at each node are plotted. The small Mach numbers in the system indicate that throughout the venting process, choking of the flow is not an issue in the relief piping. Figure 8 shows mass flow rates at each point in the system. From the figure, the transient nature of the venting process can be observed. At the beginning of the venting process, mass accumulates in the relief pipe, leading to higher mass flow rates in the downstream sections. At later times, however, a mass balance would indicate that the venting process is approaching a steady-state. Finally, Figure 9 shows the vapor fraction and the mass of hydrogen in the vacuum vessel after the rupture disk opens. The figure shows that 3 seconds after the target vessel rupture, roughly one-half of the hydrogen has been discharged from the vacuum vessel.

The remaining cases that were considered are: the system in ER-2 with the 30 psig rupture disk, the system in MPF-35 with the 20 psig rupture disk, and the system in MPF-35 with the 30 psig rupture disk. The results for each of these cases are shown with a series of graphs. For each of the three remaining simulations, we show hydrogen pressure and Mach number at each point in the system, as well as the hydrogen mass and the vapor fraction in the vacuum vessel. The results for the system in ER-2 after the 30 psig rupture disk opens are shown in Figure 10. Figure 11 presents the results for the system installed in MPF-35 after the 20 psig rupture disk opens. Finally, Figure 12 shows the results for the system installed in MPF-35 after the 30 psig rupture disk opens. In each case, we find that the pressure in the vacuum vessel decreases as soon as the burst pressure of the rupture disk is reached and hydrogen is allowed to flow through the relief line. In addition, the hydrogen velocity in the relief piping is never large enough to cause choking. These results would indicate, once again, that the relief piping is sized large enough to accommodate the hydrogen discharge after a target vessel rupture.

VII. Conclusions

A transient numerical analysis of the hydrogen discharge from the vacuum space surrounding the NPDGamma LH2 target vessel after a target vessel failure has been presented. In the analysis, conservative assumptions that will overestimate the pressure in the vacuum vessel during the venting process have been used. For example, surface temperatures and heat transfer coefficients in the vacuum vessel and relief piping have been chosen to overestimate the heat transfer rate to the hydrogen. In addition, rather than using the manufacturer's reported value for the flow resistance through the rupture disk, a more conservative value suggested by the ASME standard has been used. With these conservative assumptions, the analysis shows that as soon as the burst pressure of the rupture disk is reached, the pressure in the vacuum vessel decreases. This result indicates that the relief piping is properly sized to prevent excessive pressure levels in the vacuum vessel after a failure of the LH2 target vessel.

References

1. NPDGamma Liquid Hydrogen Target Engineering Document, v. 1, November 30, 2004.
www.iucf.indiana.edu/U/lh2target/export-files/
2. R. W. Fox and A. T. McDonald, *Introduction to Fluid Mechanics*, 4th edition, John Wiley & Sons, New York, 1992, Ch. 8.
3. Fike (www.fike.com), Technical Bulletin TB8104, December 1999. Referenced in: P. Leckner, "Rupture Disks for Process Engineers – Part 2," www.cheresources.com.
4. American Society of Mechanical Engineers, *Boiler and Pressure Vessel Code*, Section VIII, Division 1, UG131 (k), 1998, pg. 100.
5. R. B. Bird, W. E. Stewart, and E. N. Lightfoot, *Transport Phenomena*, 2nd edition, John Wiley & Sons, New York, 2002, Ch. 15.
6. K. C. Karki and S. V. Patankar, "Pressure Based Calculation Procedure for Viscous Flows at All Speeds in Arbitrary Configurations," *AIAA Journal*, vol. 27, no. 9, 1989, pgs. 1167-1174.
7. P. K. Swamee and A. K. Jain, "Explicit Equations for Pipe-Flow Problems," *Proceedings of the ASCE, Journal of the Hydraulics Division*, vol. 102, HY5, May 1976, pgs. 657-664.
8. Y. A. Cengel, *Heat Transfer: A Practical Approach*, McGraw-Hill, Boston, 1997, pg. 382.
9. Engineering Equation Solver, v. 6.728, F-Chart Software, Madison, WI. www.fChart.com.
10. R. T. Jacobsen, S. G. Penoncello and E. W. Lemmon, *Thermodynamic Properties of Cryogenic Fluids*, Plenum Press, ISBN 0-306-45522-6, 1997.
11. R. D. McCarty, "Hydrogen, Technological Survey - Thermophysical Properties," NASA SP-3089, National Aeronautics and Space Administration, 1975.

Distribution

ESA-AET file

Table and Figure Captions

Table 1. Relief line geometry for the system installed in MPF-35 and for the system in ER-2.

Figure 1. Geometry used to model the hydrogen discharge. The vacuum vessel is treated as one node in the model (node 1), while the relief pipe is modeled as five nodes (nodes 2 through 6).

Figure 2. Temperature-entropy diagram for hydrogen showing the isentropic expansion and constant volume heat addition processes.

Figure 3. Pressure in the vacuum vessel versus time for the constant volume heat addition process. Lines on the chart show the burst pressure of the rupture disks.

Figure 4. Vapor fraction in the vacuum vessel during the constant volume heat addition.

Figure 5. Hydrogen pressure at each node in the system installed at ER-2 after the 20 psig rupture disk opens.

Figure 6. Hydrogen temperature at each node in the system installed at ER-2 after the 20 psig rupture disk opens.

Figure 7. Mach numbers at each node in the system installed at ER-2 after the 20 psig rupture disk opens.

Figure 8. Mass flow rates at each node in the system installed at ER-2 after the 20 psig rupture disk opens.

Figure 9. Vapor fraction and hydrogen mass in the vacuum vessel for the system installed at ER-2 after the 20 psig rupture disk opens.

Figure 10. Results for the system installed at ER-2 after the 30 psig rupture disk opens. The figures show: (a) pressure and (b) Mach number at each node, and (c) vapor fraction and hydrogen mass in the vacuum vessel.

Figure 11. Results for the system installed at MPF-35 after the 20 psig rupture disk opens. The figures show: (a) pressure and (b) Mach number at each node, and (c) vapor fraction and hydrogen mass in the vacuum vessel.

Figure 12. Results for the system installed at MPF-35 after the 30 psig rupture disk opens. The figures show: (a) pressure and (b) Mach number at each node, and (c) vapor fraction and hydrogen mass in the vacuum vessel.

Table 1. Relief line geometry for the system installed in MPF-35 and for the system in ER-2.

MPF-35						
Section	Δx (ft)	D_h (in)	Δz (ft)	K	L_e/D	Components in Section*
1 to 2	0	3.375	0	0.5	0	Square-edged entrance
2 to 3	2.1	3.375	2.1	0	0	
3 to 4	0.9	4	0	2.4**	60	Rupture disk and flow through tee
4 to 5	2.5	6	0	0	600	Check valve
5 to 6	15.7	4	15.7	0	90	Flow through tee and one 90 deg. Bend
ER-2						
Section	Δx (ft)	D_h (in)	Δz (ft)	K	L_e/D	Components in Section*
1 to 2	0	3.375	0	0.5	0	Square-edged entrance
2 to 3	2.1	3.375	2.1	0	0	
3 to 4	0.9	4	0	2.4**	60	Rupture disk and flow through tee
4 to 5	30	6	0	0	630	Check valve and flow through 90 deg. bend
5 to 6	79	6	55	0	120	Flow through tee and two 90 deg. bends
* Rupture disk $K = 2.4^{**}$, Flow through tee $L_e/D = 60$, Square-edged entrance $K = 0.5$, Flow through 90 deg. bend $L_e/D = 30$, Flow through check valve $L_e/D = 600$						
** per ASME boiler and pressure vessel code						

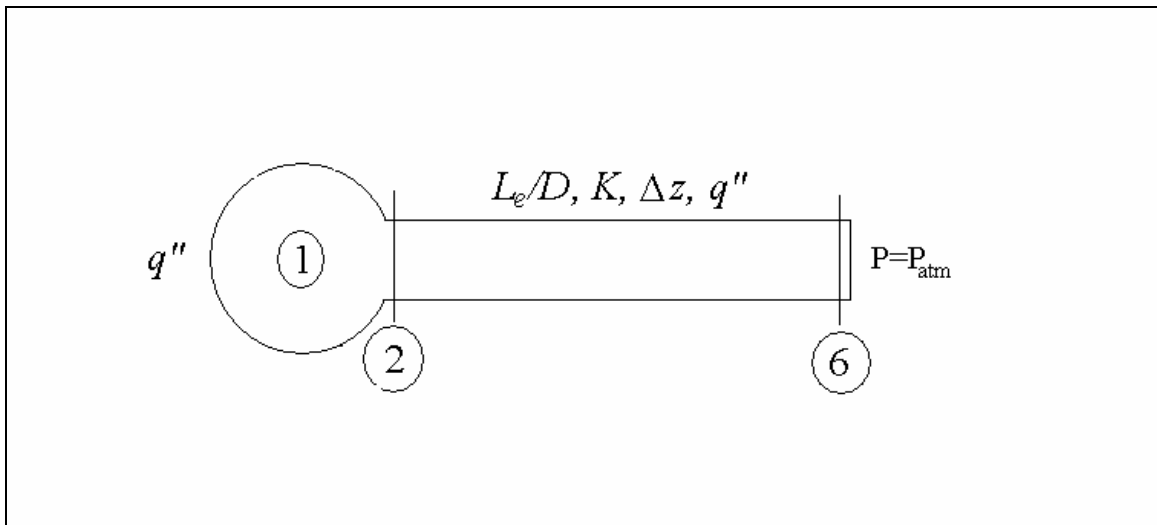


Figure 1. Geometry used to model the hydrogen discharge. The vacuum vessel is treated as one node in the model (node 1), while the relief pipe is modeled as five nodes (nodes 2 through 6).

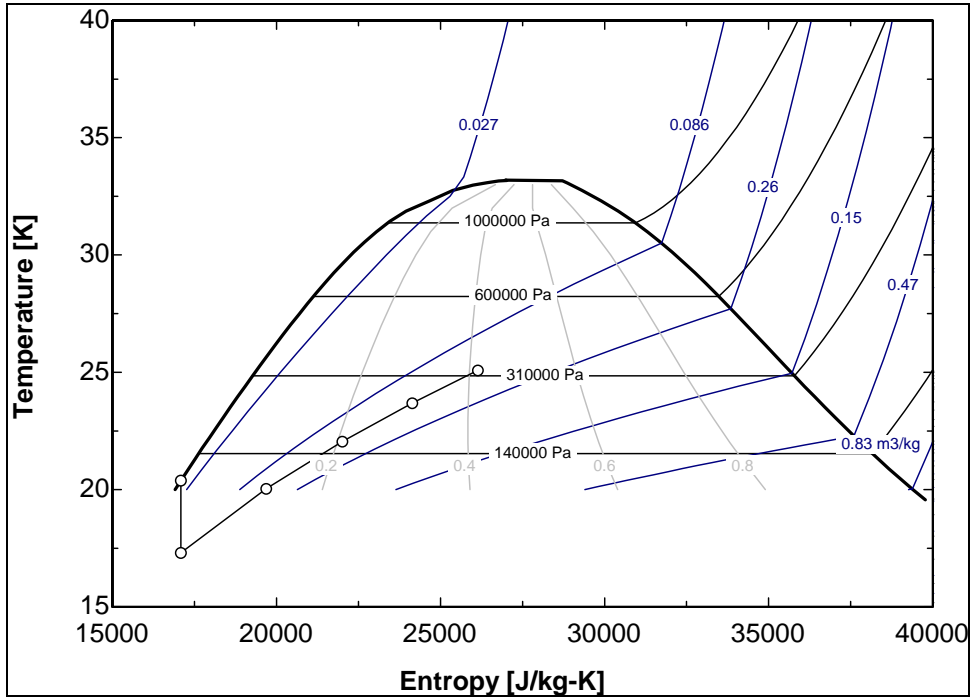


Figure 2. Temperature-entropy diagram for hydrogen showing the isentropic expansion and constant volume heat addition processes.

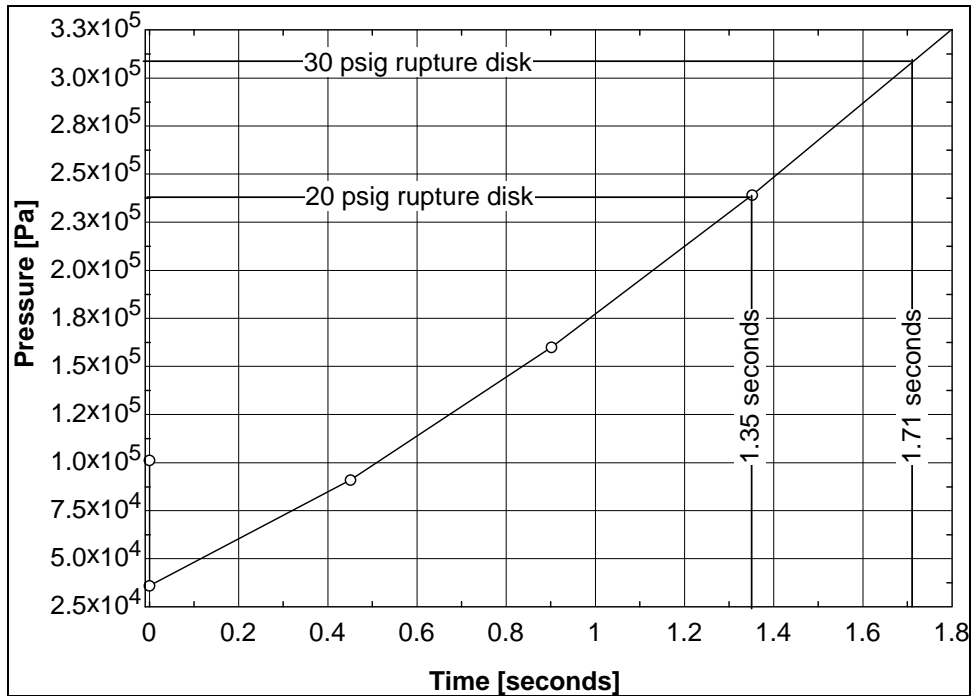


Figure 3. Pressure in the vacuum vessel versus time for the constant volume heat addition process. Lines on the chart show the burst pressure of the rupture disks.

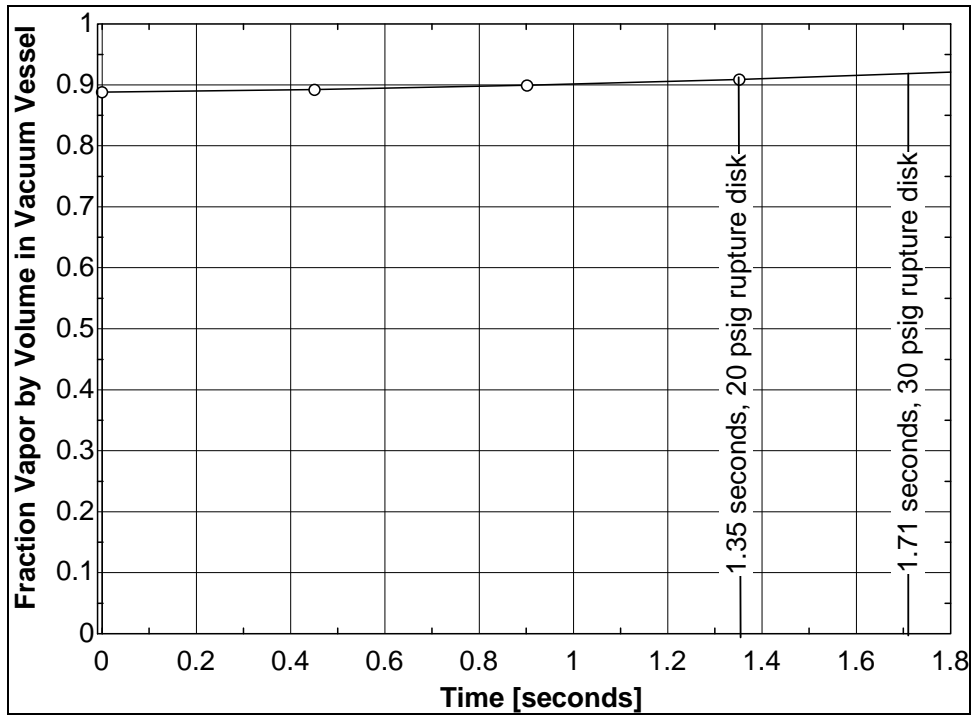


Figure 4. Vapor fraction in the vacuum vessel during the constant volume heat addition.

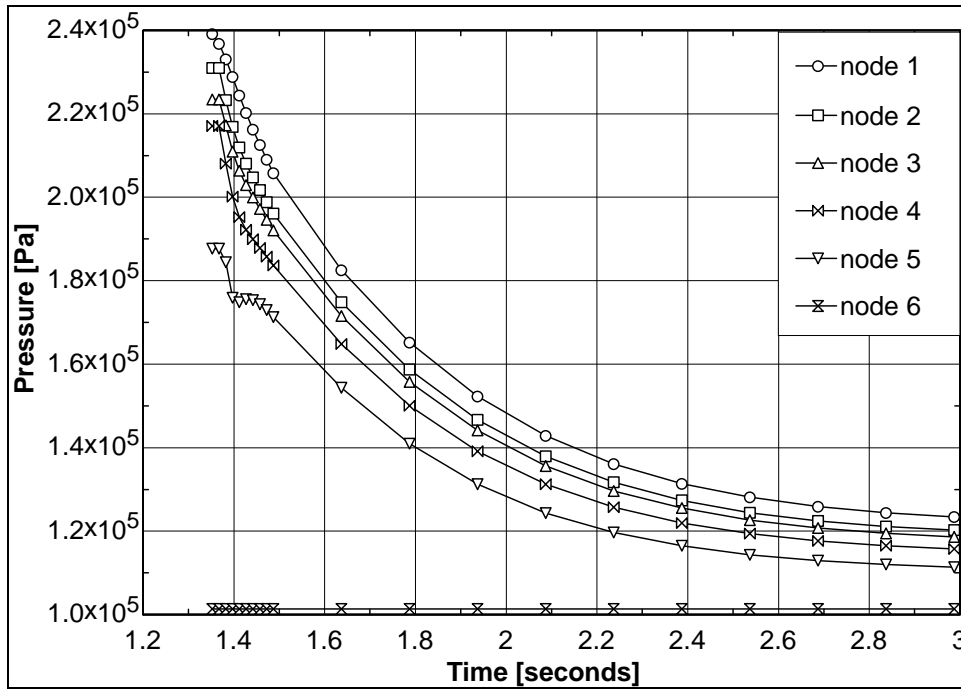


Figure 5. Hydrogen pressure at each node in the system installed at ER-2 after the 20 psig rupture disk opens.

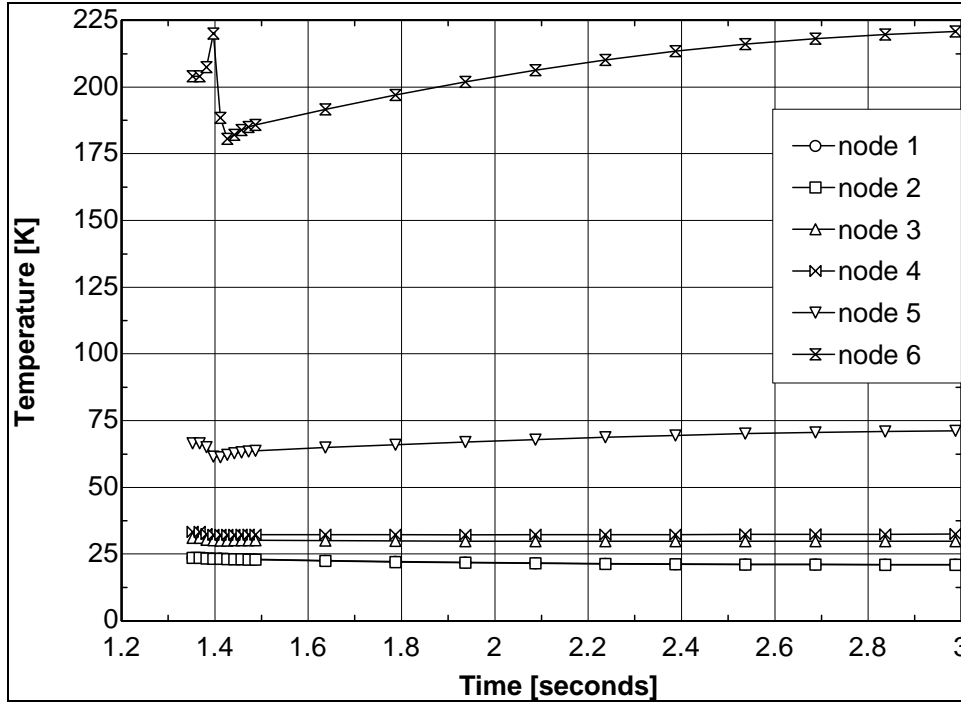


Figure 6. Hydrogen temperature at each node in the system installed at ER-2 after the 20 psig rupture disk opens.

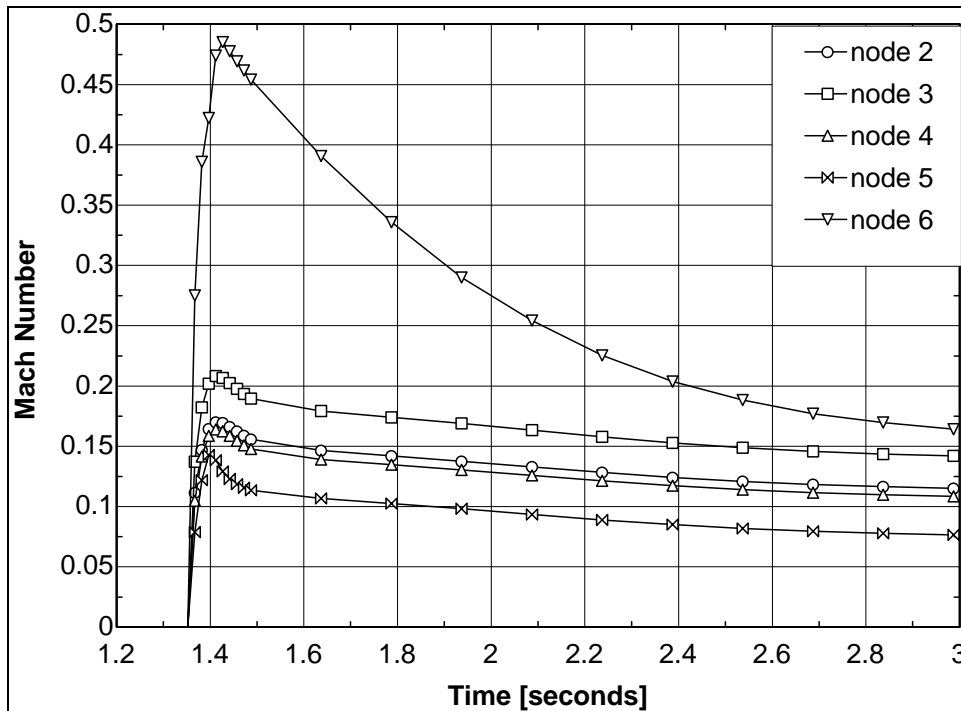


Figure 7. Mach numbers at each node in the system installed at ER-2 after the 20 psig rupture disk opens.

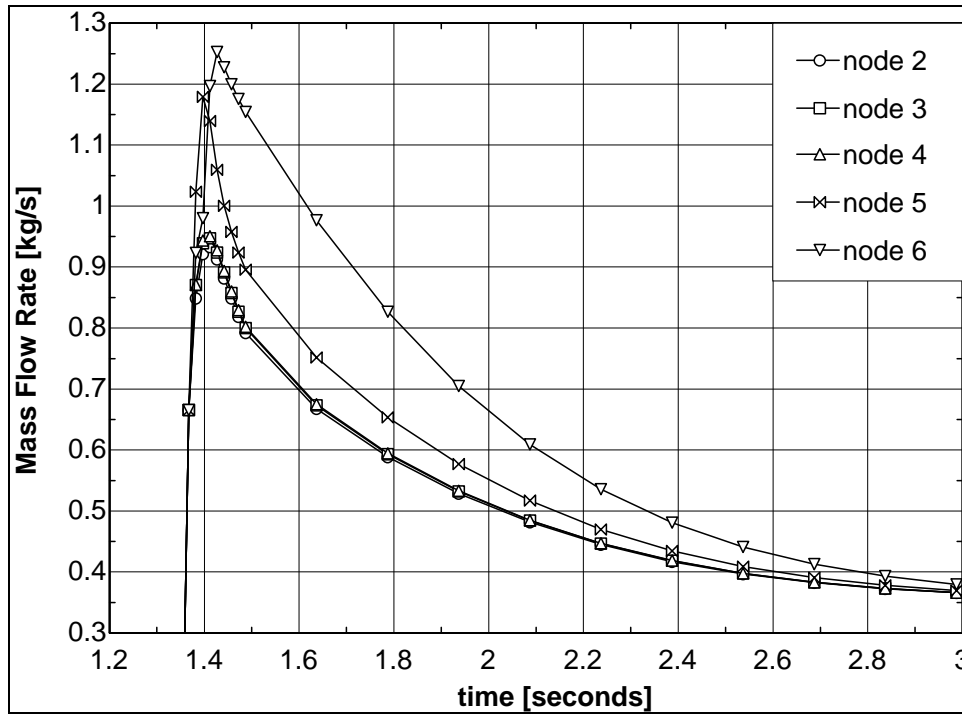


Figure 8. Mass flow rates at each node in the system installed at ER-2 after the 20 psig rupture disk opens.

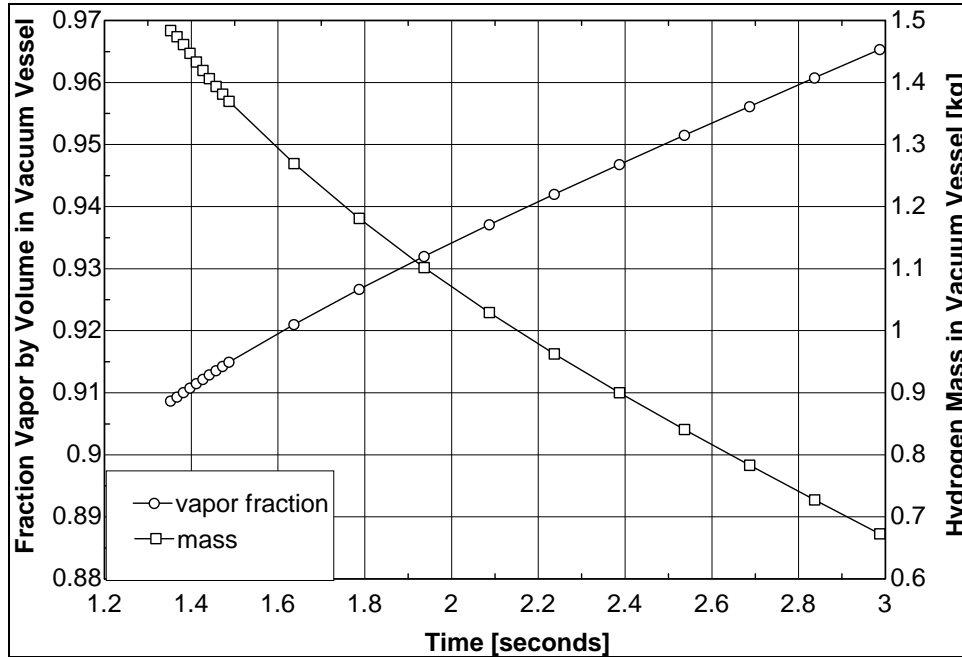


Figure 9. Vapor fraction and hydrogen mass in the vacuum vessel for the system installed at ER-2 after the 20 psig rupture disk opens.

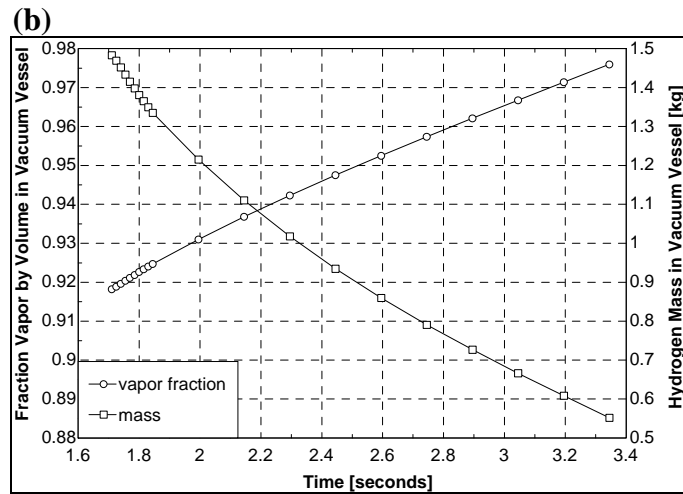
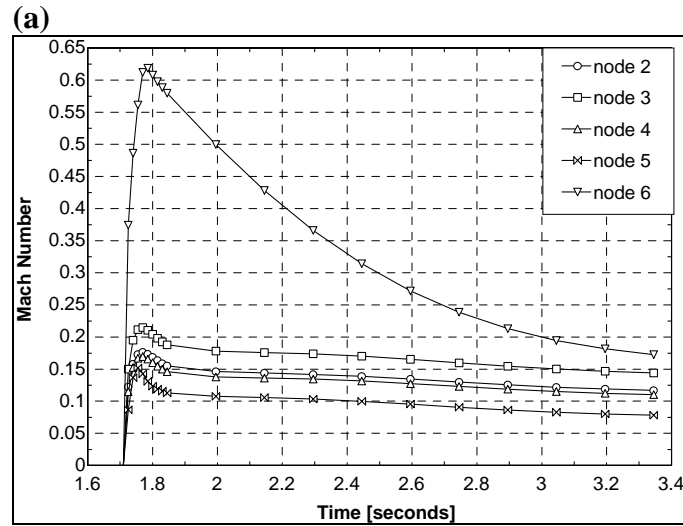
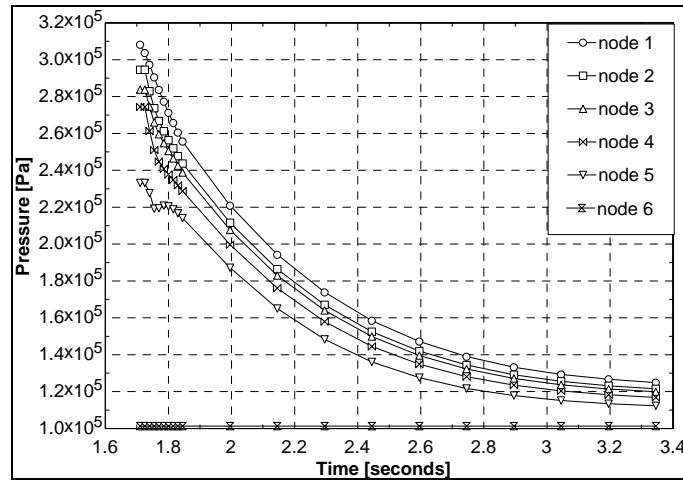


Figure 10. Results for the system installed at ER-2 after the 30 psig rupture disk opens. The figures show: (a) pressure and (b) Mach number at each node, and (c) vapor fraction and hydrogen mass in the vacuum vessel.

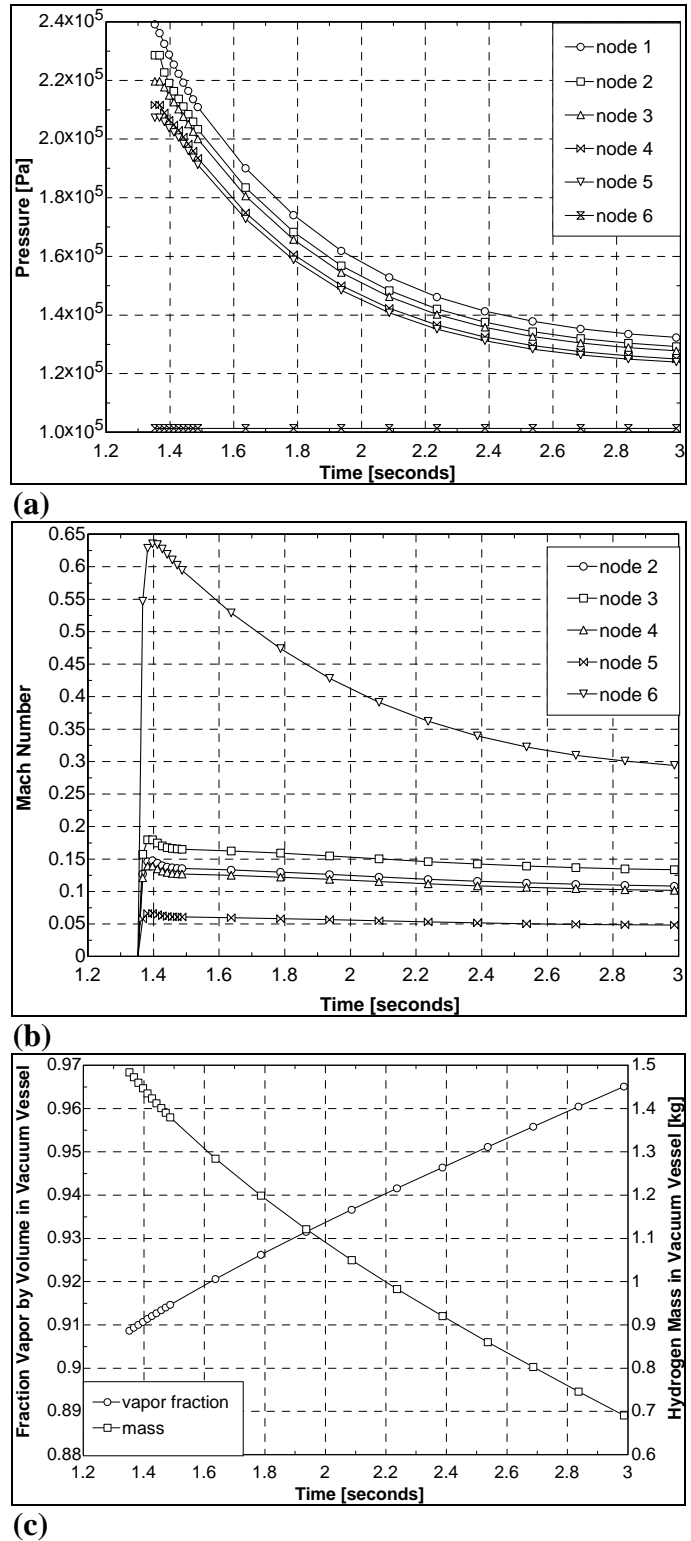
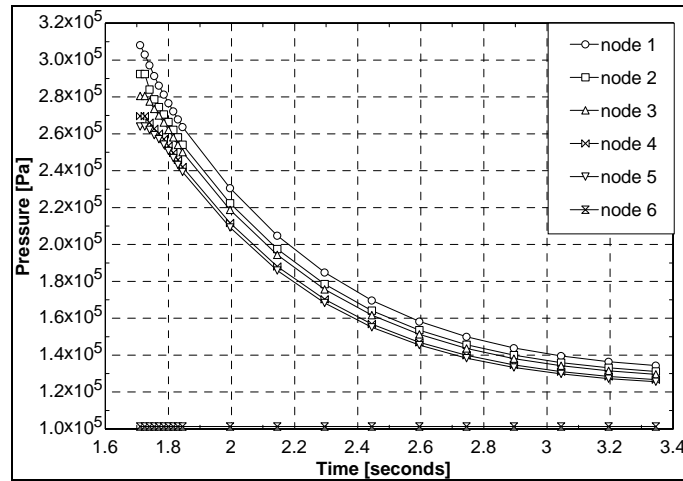
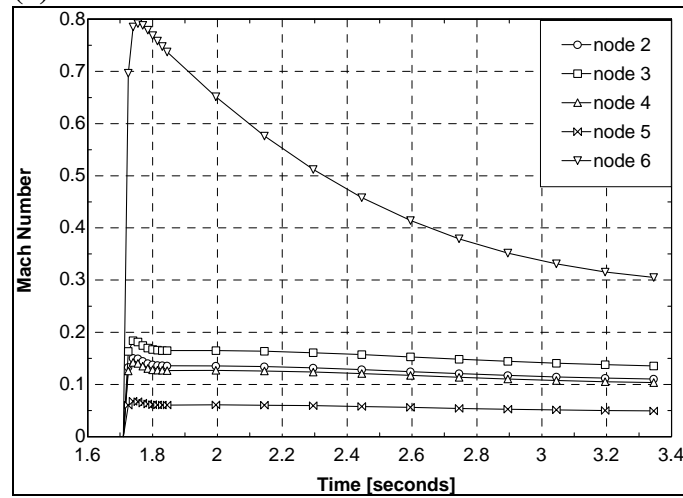


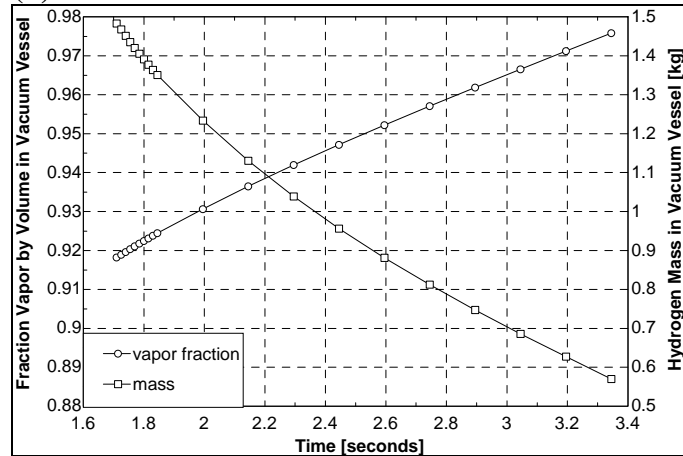
Figure 11. Results for the system installed at MPF-35 after the 20 psig rupture disk opens. The figures show: (a) pressure and (b) Mach number at each node, and (c) vapor fraction and hydrogen mass in the vacuum vessel.



(a)



(b)



(c)

Figure 12. Results for the system installed at MPF-35 after the 30 psig rupture disk opens. The figures show: (a) pressure and (b) Mach number at each node, and (c) vapor fraction and hydrogen mass in the vacuum vessel.